RSCPublishing Faraday Discussions

FD173: Effect of Post-Annealing on Plasma Etching of graphene-coated-copper

Journal:	*Faraday Discussions*
Manuscript ID:	FD-ART-05-2014-000118
Article Type:	Paper
Date Submitted by the Author:	24-May-2014

Complete List of Authors:	Hui, Lok Shu; Mcmaster University, Department of Engineering Physics Whiteway, Eric; McGill University, Department of Physics Hilke, Michael; McGill University, Department of Physics Turak, Ayse; McMaster University, Department of Engineering Physics

SCHOLARONE™
Manuscripts

RSCPublishing

ARTICLE

Effect of Post-Annealing on Plasma Etching of graphene-coated-copper

Cite this: DOI: 10.1039/

L. S. Hui [a], E. Whiteway [b], M. Hilke [b] and A. Turak [a]

Received 2014,
Accepted 2014

DOI: 10.1039/

www.rsc.org/

High temperature deposition of graphene on Cu by chemical vapor deposition can be used to produce high quality films. However, these films tend to have a non-equilibrium structure, with relatively low graphene adhesion. In this study, samples of graphene grown on copper foils by high temperature CVD were post-deposition annealed at temperatures well below the critical temperature for Cu. Resistance to etching under plasma was examined to assess the mechanical robustness of the graphene on the Cu surface, analyzed with optical and Raman microscopies. We found a correlation between post-annealing time and the etching time for complete removal of graphene from Cu. Etching rates, minimum etch times, and surface appearance were observed to vary depending on the etching plasma (air, oxygen or nitrogen). Oxygen plasmas were found to be the least aggressive, emphasizing the improved adhesion with post-annealing treatments. Our results imply that etching of graphene on Cu, and hence the adhesion of graphene, can be controlled by proper annealing and choice of plasma gas.

Introduction

Due to its chemical inertness, excellent mechanical strength, and high electrical conductivity, graphene has been a widely studied material since its discovery in 2004.[1–3] Potential applications include its use as electrodes,[4–6] charge carrier transport layers,[7–9] lubricants[10], impermeable barriers,[11,12] and nanoelectromechanical systems (NEMS).[13]

Though much research has focused on understanding the electronic and thermal properties of graphene,[1–3] the mechanical properties have been less widely explored. Recent work, however, suggests that the mechanical and friction properties of graphene are just as impressive as the electronic.[14–16] Despite the recent excellent work, there is still some controversy on the strength of adhesion of chemical vapor deposition (CVD) graphene, especially on Cu surfaces.[17–19] CVD is an excellent low cost method of producing large area graphene with controlled thickness and high quality[20,21]

Though the film quality is high, CVD graphene grown on Cu foil at high deposition temperatures (>1000°C) tends to have a non-equilibrium structure,[22] characterized by wrinkles and folds.[17,23,24,22] Deposition at high temperatures leads to rapid contraction of the graphene upon cooling[22,25,24] due to the mismatch in the thermal expansion coefficients between Cu and graphene.[26,27] The Chen group[28,29] have recently used high temperature post-deposition annealing to recover the crystallinity of the Cu surface, recovering the equilibrium structure of graphene on Cu.[23] The equilibrium structure has been found to have much higher adhesion energies [18] than that found on wrinkled samples.[17]

This study examined the impact of post-deposition annealing (post-annealing) on the graphene-Cu system when exposed to etching plasmas. Post-deposition aannealing, even at modest temperatures (<200°C), appears to be key in manipulating the adhesion strength of graphene on Cu, reflected by the increased etching times to completely remove CVD graphene from the Cu surface. Plasma etching, therefore, may be an easy and effective method of examining the impact of post-deposition treatments on graphene systems.

Experimental

Graphene was synthesized by chemical vapour deposition (CVD) on commercially available 25µm copper foils (Alfa Aesar). The foils were first chemically treated with acetic acid and annealed for 4 hours at 1078˚C under a flow of 8 sccm hydrogen gas in order to prepare the copper surface. The temperature was maintained at 1078˚C during a 4min CVD growth phase where gas flows of 1.2 sccm methane was introduced. Long annealing time and short growth period were chosen in order to limit the size and density of the graphene domains. To observe the graphene flakes, oxidation of the Cu surface is necessary to provide contrast between the graphene coated and uncoated portions of the Cu surface. Samples were annealed in a batch on a hot plate (Pace Heat Wave) in air at

This journal is © The Royal Society of Chemistry 2014

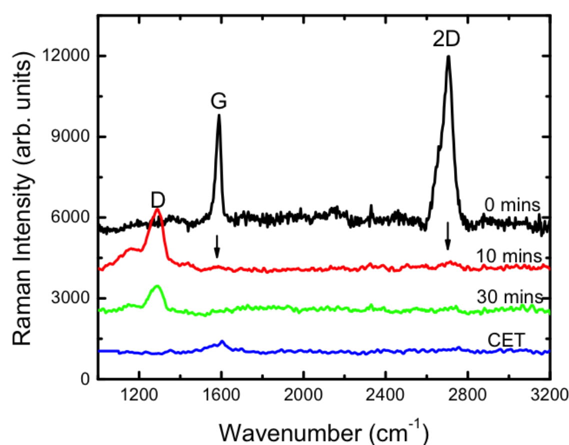

Figure 1 Raman spectra for CVD graphene on Cu foil at etching times of 0, 10, 20 and 201(CET) min, showing the evolution of the etching process for O_2 plasmas. The critical etching time is defined as the complete removal of graphene, as determined by optical methods.

180℃ with different annealing times ranging from t=2, 4, 9, 15, 30, 60 min. The groups of samples with different annealing times were then separated into batches for air (unfiltered laboratory air), nitrogen (Alphagaz, 99.999%) and oxygen (Alphagaz, 99.999%) plasma etching. The plasma etching was performed in a Harrick Plasma PDC-001 plasma cleaner system and Thierry Plasma Zepto Low Pressure System with 13.56MHz R.F. generator at 29.6W. The plasma chamber was held at a base pressure of 70mTorr prior to target gas filling. During etching, a gas flow rate of 30 sccm was maintained. The samples were progressively etched from 2-260min with time intervals of minimum 1min and were observed under an optical microscope (Leica DMR microscope) to detect the first disappearance of contrast. For the case of N_2 plasma etching, a second post-annealing step of the etched samples was needed to show contrast of Cu-graphene after treatment. The time intervals from the etching are accumulated to determine the minimum time required to completely remove the graphene from the Cu surface, designated as the critical etching time. Raman spectra were collected using a Renishaw inVia spectrometer at 514nm laser excitation, with a 20x objective and 1200 l/mm grating. The laser power was 20mW, to prevent damage to the graphene. All spectra were background corrected to remove the Cu photoluminescence excited at 514nm[30] (see supplementary information).

Results and discussion

Though exposure to plasma is often used to modify the electronic properties of graphene layers,[31–35] under sufficiently high doses, bombardment with the energetic particles can also completely etch away the graphene layer. The etching time for complete removal of any residue is generally correlated to the strength of the adhesion of the coating on the surface.[36] Therefore, plasma interactions are a potential method of probing the mechanical strength of graphene-copper interfaces. As our interest concerns the robustness of the graphene against plasma etching, partially covered substrates were desired. The CVD process was tuned to produce square graphene flakes on the Cu foil with ~30-100μm widths.

Impact of etching times

Figure 1 shows the Raman spectra for as-grown graphene, and the resultant spectra after etching in O_2 for various times. The pristine samples show both the characteristic features for graphene, the G and 2D peaks at 1587 cm^{-1} and 2705 cm^{-1} respectively. The G peak corresponds to the first order degenerate phonon energy, E_{2g} mode at the Γ point of graphene;[37] the sharp 2D peak is a result of the second order phonon intervalley scattering, from the π–π* transition.[37–39] The absence of a peak between ~1280-1350cm^{-1} suggests that the graphene islands are mostly defect free.[37,40] The $I_G/I_{2D\ (peak\ height)}$ ratio of 0.4 indicates that the graphene flakes on the Cu surface are mostly few or even single layer.[37,41] The 2D peak can be fit by a single Lorentzian (not shown), further supporting the idea that the CVD grown graphene films are mostly single layer, defect free patches on the Cu surface.[37] Some islands were also observed with slightly higher I_G/I_{2D} ratios and a shoulder on the 2D peak, suggesting some flakes are likely multilayered.[37]

After a short etch in O_2 plasma, significant sp^3 defects are introduced with a strong D band appearing at 1290cm^{-1}.[37,42] Though much reduced, both the G and 2D bands are still barely visible as shown by the arrows in Figure 1. There may also be a merging of G and D' broad band at 1590cm^{-1}, which is attributed to the C-H sp^3 hybridization defect and the overtone of D mode activated after plasma treatment [23,28] These changes suggest that the plasma initially introduces defects into the graphene rather than removing it, as is often seen in lower dose plasma processing used to tune the electronic configuration of graphene flakes.[31] Another explanation for the appearance of the strong D band is the formation of graphene oxide, though that is generally accompanied by an equally large G peak.[43] Further etching eliminates the G, D' and 2D signals and reduces the scattering intensity of the D band, indicating that graphene/graphene oxide is being removed from the surface. Finally, after the critical etching time (CET), there is no more evidence of graphene in the Raman spectrum. This fully etched condition of the graphene was determined by optical microscopy.

As received, the graphene on Cu foil is without any contrast in the forward scattering condition. Cu, however, is prone to oxidation in air even at low temperatures. Graphene has been widely reported as an excellent passivation layer,[11,12] protecting the surface from chemical oxidation as the densely packed benzene-ring structure makes graphene impermeable to most gases, including helium.[44,45] Mild oxidation, from short post-annealing treatments in air or even exposure to oxidizing plasmas, can therefore be used to visualize the graphene islands (see Figure 2(a)). The contrast results from the different light scattering intensity and refractive indicies of cuprous oxide and the unoxidized Cu protected under the graphene. The oxidation contrast, therefore, can be used as a method of tracking the progress of etching. Figure 2 shows the effect of the etching procedure on the graphene islands, supporting the findings suggested by the Raman data. After short etching times, the graphene is still visible, then becomes progressively less visible as etching progresses. Finally, the critical etching time (CET) is determined as the point where almost no contrast is visible after

 This journal is © The Royal Society of Chemistry 2014

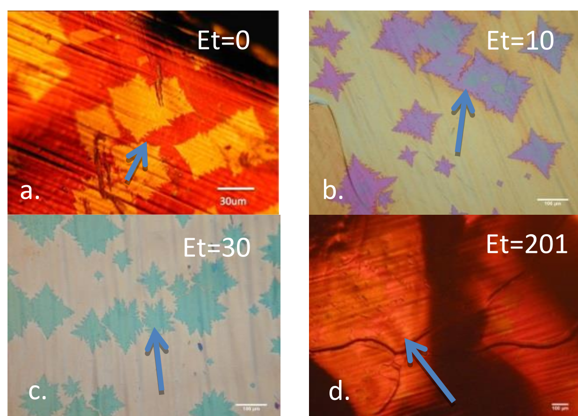

Figure 2 Optical micrographs of CVD graphene on Cu foils. (a) As-grown samples, annealed to show contrast between bare and graphene covered regions (b-d) same sample after etching in O_2 plasma for 10, 30 and 201min. Etching time is denoted as "et" in the figures. Blue arrows indicate the contrast showing the graphene islands. The final panel was used to determine the critical etching time (CET).

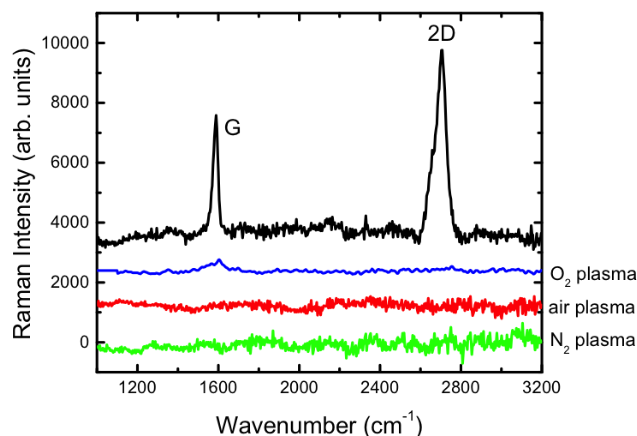

Figure 3 Raman spectra of as-grown CVD graphene on Cu and after etching with different gases.

etching, suggesting complete removal of the graphene layer (Figure 2(d)).

After CET, there is still a Raman feature visible at the G/D' location of ~1580cm^{-1} (Figure 1). However, the eigenvector of the G mode involves the in-plane bond-stretching motion of pairs of C *sp*^{2} atoms, and does not require the presence of six-fold rings.[46]Without the accompanying 2D peak, which needs six-fold rings to be excited [46], this cannot be taken as a feature of graphene, and is most likely due to C=C residue on the surface. As can be seen in Figure 3, after the CET as determined from optical observations, Raman measurements show no indication of graphene on the surface for N_2, O_2 and unfiltered laboratory air etching plasmas. This suggests that the optical method is adequate to determine the CET for complete removal of graphene from the Cu surface, and the CET can be considered to be roughly proportional to the strength of the interaction between graphene and the Cu surface. Optical determination of CET is straight-forward for O_2 and air plasmas, as exposure to the plasma also oxidized the Cu surface; however, identification of N_2 CET required a post-etching anneal of the etched samples to show contrast of Cu-graphene after treatment. It is likely therefore that the visual method leads to an over estimation of the real CET for N_2 plasmas. This was confirmed with Raman measurements where graphene patches were visible optically, but there was no signature of graphene (see next sections).

Effect of post-deposition annealing

CVD graphene grown on Cu foil, at high deposition temperatures, such as those in this study, tend to have a non-equilibrium structure.[22] Egberts et al [17] recently showed that the work of adhesion for graphene on Cu is low for such systems. The Chen group [28,29] have been able to use high temperature post deposition annealing to recover the crystallinity of the Cu surface, approaching the equilibrium structure of graphene on Cu.[23] High quality equilibrium films have been reported to have very high adhesion strengths.[18] This suggests that post-deposition annealing might increase the interaction strength between graphene and Cu.

To examine this effect, we performed low temperature (180°C) post-deposition annealing on our graphene-Cu samples for various annealing times. As described above, short annealing times can make visible the graphene islands. Under further annealing (Figure 4(b)) the contrast increases, likely due to the enhanced oxidation ofunprotected Cu in the presence of graphene, recently described by Zhou et al.[10] Eventually, after 60min annealing, in some areas of the sample, the graphene islands edges are no longer clear, and the islands appear damaged. This is a likely result of graphene exfoliating from the surface, due to a mismatch in the thermal expansion coefficient of graphene ((-8.0±0.7)x10^{-6} K^{-1}) and the Cu crystals (14x10^{-6} K^{-1}).[26,27] With longer annealing time, more material is allowed to expand and the rigid graphene structure is not fully bonded to the surface, exposing some of the Cu underneath the surface, resulting in a more "messy" oxidation of the Cu foil[47].

Figure 5 shows the Raman spectra for the post-deposition annealed films. In all cases, the G and 2D bands are both visible, without D band development. This suggests that there was neither significant defect nor graphene oxide formation.[43,48] Post-deposition annealing in fact seems to have very little impact on the graphene islands, even when optically significant damage appears to have occurred. The only notable change is a slight blue shift of the 2D band observed to occur systematically with annealing time. Though this is characteristic of multilayer graphene,[49] no peak broadening or change in I_G/I_{2D} ratio (varies between 0.36-0.46 depending on graphene flake) was observed. The observed features can be well fitted with a single Lorentzian peak shape with similar full width at half maximum (FWHM), pointing to defect free, monolayer graphene in all cases. Another possible explanation for the observed shift is the build up of strain at the interface. Wang et. al. [50] saw shifts in the 2D band resulting from the lattice mismatch between SiC and carbon layer/buffer layer, which has a graphene-like honeycomb lattice that is covalently bonded to the SiC substrate [50]. A change in the mechanical interaction between the

RSCPublishing

ARTICLE

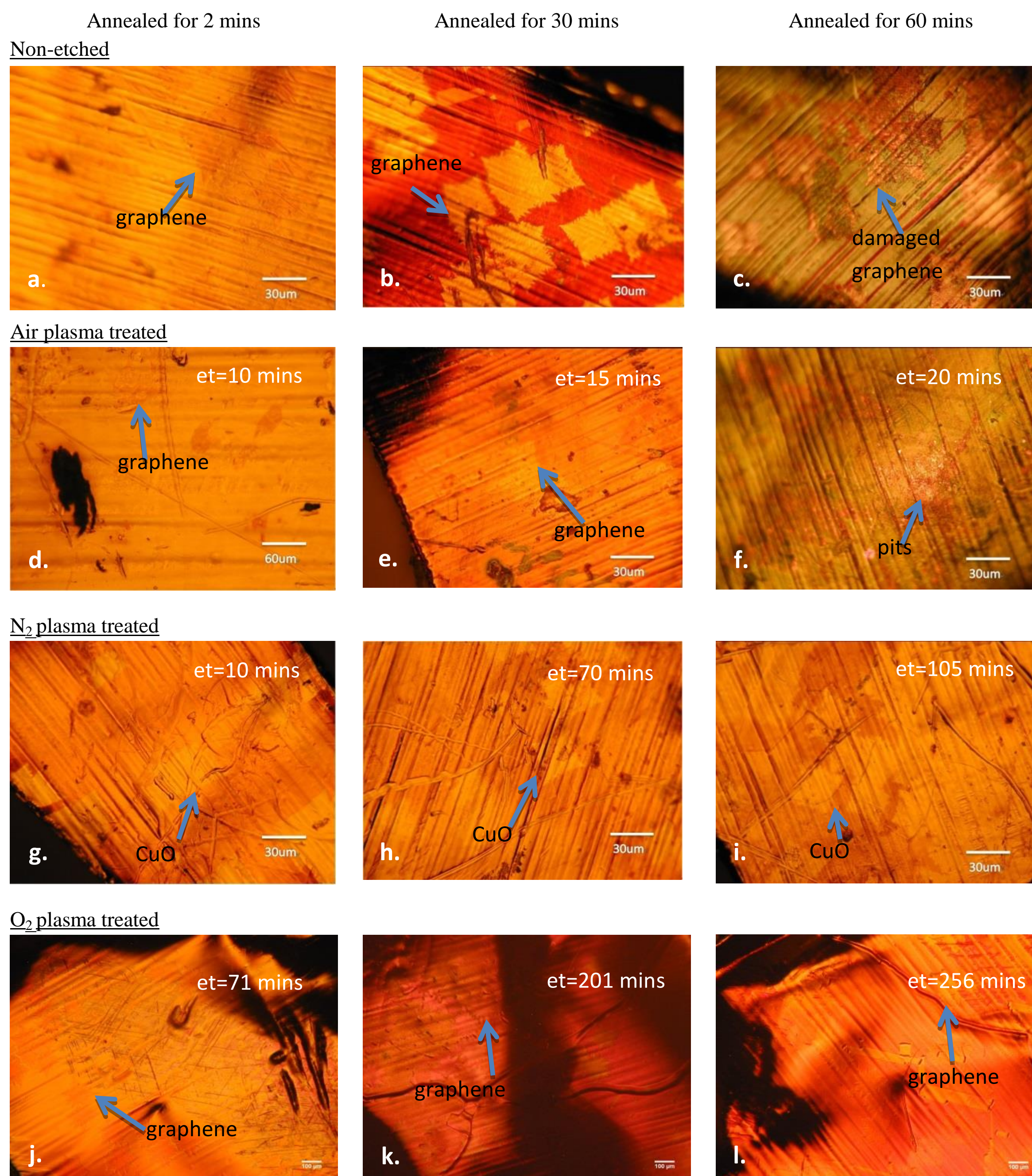

Figure 4 (a.-l.) Optical micrographs of CVD graphene on Cu foil annealed and etched for various times. (a, d&g) samples post-annealed for 2 min.; (b, e&h) for 30 min. and (c,f&i) for 60 min. (a-c) samples have not been plasma treated; (d-f) treated with air plasma, (g-i) N_2 plasma treated and (h-l) O_2 plasma treated with the etching time denoted as "et" in the figures. Blue arrows indicate the contrast showing the graphene islands.

RSCPublishing

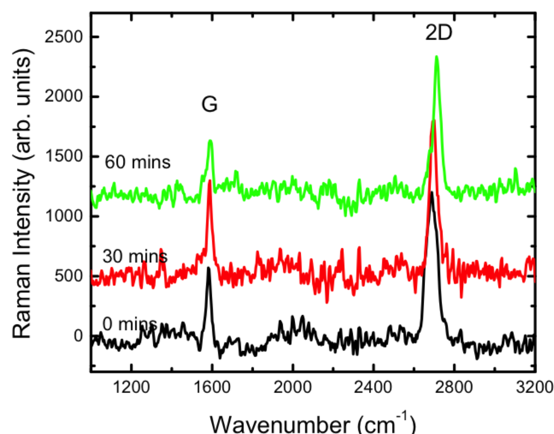

Figure 5 The Raman spectra of CVD graphene on Cu samples with different post-annealing times at 180°C (0,30&60 min). The spectra were normalized to the 2D peak at ~2700cm^{-1} intensity for comparison.

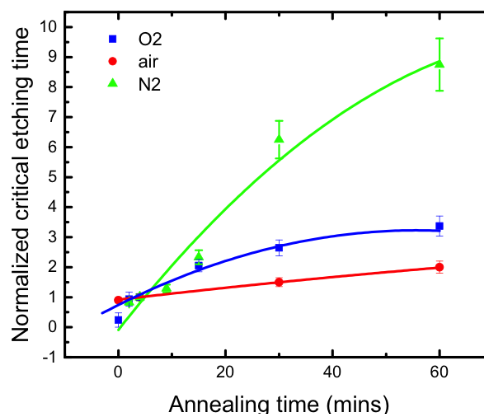

Figure 6 Normalized CET for graphene with different post-annealing treatment for various plasmas. Lines are least squares fit on data. The CET have been normalized using to the value of annealing time at 4 min, where contrast is visible, to eliminate possible sample discrepancies and emphasize the common trend for all process gases.

graphene and Cu could also lead to a build-up of strain at the interface.

Upon exposure to plasma, however, significant differences were observed with the post-annealing time. Optically, as can be seen in Figure 4, systematically longer etching times were necessary to fully remove the graphene from the substrate with post-annealing, for all etching gases. The observed CET for all the process gases are summarized in Figure 6. In all cases, increased annealing time protects the system against etching. The visually different etching times as a function of annealing, as shown in Figure 4(d,e&f), (g,h&i) and (j,k&l) support the premise that annealing can be used to control the removal of graphene, by making the structure more robust. It takes much longer in all cases to see complete removal of the graphene from the surface. Figure 7 shows the Raman spectra for the optically determined CET for O_2 plasma with various post-annealing times. Though there is no evidence of graphene or even C residue on the as-grown samples, even short post-deposition annealing changed the resultant spectra. With only 2min of annealing, the defect or graphene oxide D band observed previously with 10min plasma exposure was still visible after 75min plasma exposure (see supplementary information for non-normalized CET values). Further annealing shows increasing signal from the G/D' band, which may be due to C=C residues that are not removed even with extremely long etch times (250min etching for 60min post-annealing time). The extremely long etching times, and the inability of the plasma to remove carbon residues indicates a strong interaction between the Cu and the graphene.

Effect of plasma gas

Though Figure 6 shows that the trend of increasing CET with annealing holds for all process gases, there are significant differences in the measured CET times for the different etch gases. These effects are visible even with normalization to remove sample variations. Using the CET estimations, air is the most aggressive etchant, with O_2 and N_2 plasmas having decreasing aggressiveness. The effect of post-annealing in protecting the graphene from etch removal is greatly enhanced the less aggressive the etchant. However, the optical measurements are slightly misleading. Raman measurements for the same etching time, shown in Figure 8, support the order of the O_2 and air plasmas, but completely contradict the behavior with N_2 etching.

Figure 8 does confirm that the different process gases have different impacts on the graphene for the same etching time. In this case, N_2 plasmas appear to be the most aggressive. No Raman signal is visible from graphene nor are there any C-O, C=O bands after 10min etching, suggesting a total destruction of graphene and carbon residues. N_2 plasma etching is a physical sputtering process, that has previously been used for nitrogen doping of graphene[51] and is thought to lead to unsaturated dangling carbon bonds at the graphene edges.[51] The dangling carbon bonds can react with oxygen atoms once it is exposed in air. However, in this study, no evidence of graphene or graphene oxide was observed, only complete sputter removal of the graphene.

It appears that, while the optical detection for determining the CET works well for air and oxygen plasmas, values of the CET as determined optically are highly overestimated for N_2. Optically, Figure 4(h) shows that the contrast initially assigned to graphene is still visible for a sample that has been etched for 75 min, under the same annealing conditions as the 10min etching in Figure 8. As nitrogen plasma cannot oxidize the Cu during etching, this contrast is more likely to result from the varying degree of Cu oxidation rather than a signature of graphene on the surface. The first

This journal is © The Royal Society of Chemistry 2014

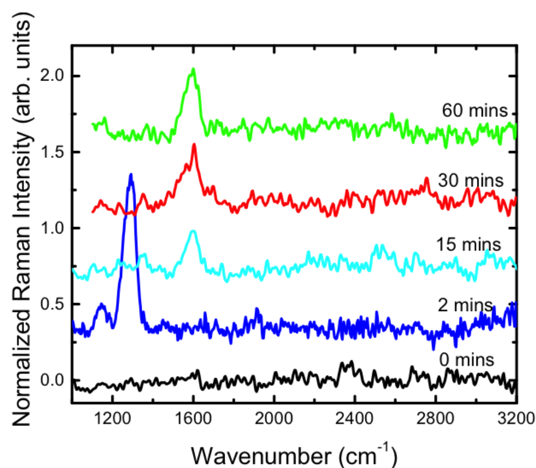

Figure 7 Raman spectra for CET on CVD graphene on Cu foils with O_2 plasma for various post-annealing times (0-60min) at 180ºC.

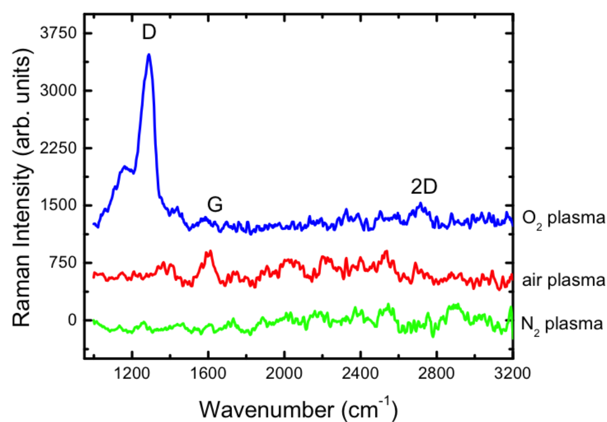

Figure 8 Raman spectra for CVD graphene on Cu foils with the same post-annealing (30 min) and etching times (10 min) with different gases.

annealing step oxidizes the regions without graphene. After interaction with the plasma, the graphene is removed, leaving behind regions with different levels of oxidation. During low temperature oxidation, metastable Cu_3O_2 forms first followed by CuO, the thermodynamic stable phase of cuprous oxide.[52] Possibly, the regions covered with graphene form the metastable oxide during the second annealing step (i.e. after plasma etching to expose the graphene), while the previously oxidized regions continue to oxidize further. Eventually, what appears to be "fully-etched", without contrast, indicates uniform oxidation or complete removal of the initially formed oxide by the vigorous physical sputtering action of the plasma. The trend in the observed CET for N_2 plasma may suggest that it takes longer for the cuprous oxide to be sputtered away at longer annealing times.

The Raman data indicates that air plasma is also very aggressive, leaving only the C=C residue/G band at 1590cm^{-1}. Air plasma etching is a very vigorous process, with CET reached quickly with visible pitting observed on the Cu/graphene surface (see Figure 4(f)). This pitting is likely due to the effect of hydrogen plasma in air as Diankov et al.[53] has observed the high selectivity of hydrogen gas on graphene. Pits are not present on samples etched by N_2 (Figure 4 (i)) or O_2 plasma (Figure 4(l)) for the same annealing time and even for much longer etching times. It is likely that there is true etching occurring with the air plasma, due to the highly reactive O^- and H^- radicals, as well as the sputtering observed with nitrogen.

O_2 plasmas were the least aggressive, showing the defect structure, D band, with some G and 2D peaks barely visible. As described previously, there could also be a broad D' band, merging with the G. The presence of both D' and D peaks suggests significant doping and defects are introduced but likely little removal of graphene. The gas with the slowest etching rate is thus the oxygen plasma, where only chemical etching takes place with O^- radical species.

The rates observed for the various plasmas can be attributed to the mechanisms of plasma etching for the different gases. Different plasma gases can have varied interaction mechanisms and diverse ions in the plasma.[53–55] Plasma is ignited by the large voltage applied across the electrodes outside the plasma chamber, which causes the free electrons to accelerate rapidly towards the anode. When the electrons collide inelastically with the gas molecules, an electron will be removed from the molecules and thus the gas will then be dissociated or ionized. The removed electron continues to be accelerated to the anode and collides with other gas molecules, resulting in a cascading effect. The gas discharge causes excitation and relaxation of gas molecules that releases energy in the form of photons and thus causes the glow inside the chamber.

The process of etching is generally considered that which results from radicals actively breaking the chemical bonding and reacting with the substrate surface.[56] Ions, however, can also cause energetic bombardment or ejection of atoms from the surface, a process referred to as sputtering. Oxygen will form highly reactive radicals by molecule dissociation, resulting in an etching of the graphene, while nitrogen can be ionized and form ions,[57–59] removing graphene primarily through sputtering. Under exposure to air plasma, graphene is expected to be both etched and sputtered by oxygen, hydrogen, nitrogen, carbon and other atoms of trace gases present in air.[55] As there is high concentration of 78% of nitrogen in air, one might expect the air plasma etching process to be dominated by nitrogen. However, pure N_2 plasma showed a much faster etching compared to air and oxygen plasmas.

Possible mechanisms for increased adhesion strength with annealing

The time for complete removal of any residue is generally correlated to the strength of the adhesion of the coating on the surface.[36] The observed increase in the CET with annealing for Cu-graphene systems, therefore, suggests significant improvement in the interaction between graphene and Cu, and an improvement in the mechanical properties of the interface. There is some controversy in the literature regarding the value of the adhesion strength between graphene and Cu,[17–19] and on the nature of the interaction leading to this value.

 This journal is © The Royal Society of Chemistry 2014

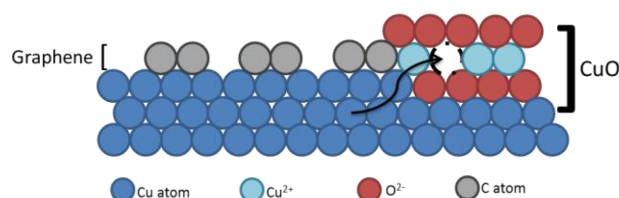

Figure 9 Schematic of graphene-Cu interface oxidation

There are two main mechanisms that might be used to describe the observed behavior with plasma etching of the graphene-Cu interface: the process of Cu oxidation itself, or the reconstruction of the Cu surface with annealing.

The CET as determined for N_2 etching seems to be due to the removal of Cu oxides rather than the graphene layer. Yet, the trend of increasing resistance to etch removal with annealing is observed. As Cu is highly susceptible to oxidation, even at low temperatures, it may be that the oxidation process itself leads to the increased strength of the interaction between Cu and graphene.

Fundamentally, the oxidation of Cu can be described by the Cabrera-Mott theory.[60] Cu ions and electrons migrate to form the oxide layer on the surface, leaving cationic Cu sites behind.[61] The strong electric field that results promotes further diffusion of Cu ions to continue oxidation.[61]

In the composite Cu-graphene system, prolonged annealing may provide more kinetic energy for Cu ion migration to areas where graphene is absent (Figure 9). As the vacant Cu cation sites draw Cu ions to the oxide-metal interface, they may pile up under the graphene flake. This could result in a stronger coupling of C-π orbitals and Cu d-orbitals hybridization of the graphene-Cu interface. This bunching of the Cu under the graphene layers as a result of the oxidation electric field could explain the blue shift observed in the 2D band with annealing (see Figure 5), previously attributed to interfacial strain [50].

Another possible mechanism influencing the etch resistance of the post-annealed system is the surface reconstruction of the Cu due to annealing. Rapid contraction of the graphene upon cooling is observed with high temperature (>1000°C) graphene deposition[22,25,24] due to the mismatch in the thermal expansion coefficients.[26,27] This is one of the possible mechanisms for the formation of wrinkles widely observed in graphene-Cu systems.[22,17,23,24] Cho et al and Tian et al.[28,29] have seen that high temperature post-annealing is able to partially heal the non-equilibrium structure that results from high temperature growth. Zhang et al.[22] saw that the existence of steps in Cu under the graphene lowers the adhesion. With annealing induced reconstruction recovering the steps within a Cu grain[28] the graphene wrinkles could relax, recovering the Moiré reconstruction pattern[23]. In the equilibrium structure, graphene is unwrinkled, and flat graphene flakes are likely to have higher adhesion to the surface compared to wrinkled ones.[18,62] The observed blue shift, attributed to interfacial strain [50], could also result in this case, where the lattice mismatch in changed by the reconstruction of the Cu surface. Though we use lower temperatures for our post-annealing study, it is possible that a similar, though incomplete, reconstruction is occurring in our samples. The increase in interaction strength, as suggested by the robustness to etching, with annealing time therefore could be correlated to the amount of reconstruction.

Further work using friction measurements to clarify these mechanisms is currently under way.

Conclusions

The graphene grown on Cu foil by high temperature CVD was annealed after deposition, and exposed to various plasmas. The post-annealing treatment alters the mechanical strength of graphene adhering on the Cu foil, as shown by the increased resistance to plasma etching. Raman spectroscopy confirms that the graphene is damaged after the annealing and plasma treatments, but typically not oxidized during these treatments. The samples were etched and sputtered by air, oxygen, and nitrogen plasmas, yielding different etch rates and appearance and uniformity of the graphene. Nitrogen plasma has a much faster etch rate than air and oxygen due to the mechanism of physical sputtering. For any given plasma however, with post-annealing before plasma exposure, the graphene is harder to remove due to the bonding between the graphene and Cu substrate. Our results imply that etching of graphene on Cu can be controlled by proper annealing and the right choice of plasma gas. Plasma etching, with suitable process gas, appears to be an effective method of estimating the impact of post-processing effects on the mechanical properties of CVD graphene.

Acknowledgements

The authors acknowledge financial support from 384889-2010 CREAT. The authors are grateful to J. Moran-Mirabal for the Harrick Plasma system, P. Jonasson for the annealing system, S. Kornic for the Raman instrument and CEDT for the microscope support at McMaster University. P. Egberts of U. Calgary is gratefully acknowledged for insightful discussions.

Notes and references

1. C. Lee, X. Wei, J. W. Kysar, and J. Hone, *Science*, 2008, **321**, 385–8.

2. Y. S. Dedkov, M. Fonin, U. Rüdiger, and C. Laubschat, *Appl. Phys. Lett.*, 2008, **93**, 022509.

3. K. S. Novoselov, a K. Geim, S. V Morozov, D. Jiang, Y. Zhang, S. V Dubonos, I. V Grigorieva, and a a Firsov, *Science*, 2004, **306**, 666–9.

4. H. Park, R. M. Howden, M. C. Barr, V. Bulovi, and P. E. T. Al, *ACS Nano*, 2012.

5. Y. Wang, S. W. Tong, X. F. Xu, B. Ozyilmaz, and K. P. Loh, *Adv. Mater.*, 2011, **23**, 1514–8.

6. Y. J. Jeong, J. Jang, S. Nam, K. Kim, L. H. Kim, S. Park, T. K. An, and C. E. Park, *ACS Appl. Mater. Interfaces*, 2014, **6**, 6816–24.

7. S. Zhong, J. Q. Zhong, H. Y. Mao, R. Wang, Y. Wang, D. C. Qi, K. P. Loh, A. T. S. Wee, Z. K. Chen, and W. Chen, *ACS Appl. Mater. Interfaces*, 2012, **4**, 3134–40.

8. M. M. Stylianakis, E. Stratakis, E. Koudoumas, E. Kymakis, and S. H. Anastasiadis, *ACS Appl. Mater. Interfaces*, 2012, **4**, 4864–70.

9. Q.-H. Wu, G. Hong, T. W. Ng, and S. T. Lee, *Appl. Phys. Lett.*, 2012, **100**, 161603.

10. D. Berman, A. Erdemir, and A. V. Sumant, *Mater. Today*, 2014, **17**, 31–42.

11. S. Chen, L. Brown, M. Levendorf, W. Cai, S.-Y. Ju, J. Edgeworth, X. Li, C. W. Magnuson, A. Velamakanni, R. D. Piner, J. Kang, J. Park, and R. S. Ruoff, *ACS Nano*, 2011, **5**, 1321–7.

12. E. Sutter, P. Albrecht, F. E. Camino, and P. Sutter, *Carbon N. Y.*, 2010, **48**, 4414–4420.

13. J. S. Bunch, A. M. van der Zande, S. S. Verbridge, I. W. Frank, D. M. Tanenbaum, J. M. Parpia, H. G. Craighead, and P. L. McEuen, *Science*, 2007, **315**, 490–3.

14. C. Lee, X. Wei, J. W. Kysar, and J. Hone, *Science*, 2008, **321**, 385–8.

15. T. Filleter, J. McChesney, a. Bostwick, E. Rotenberg, K. Emtsev, T. Seyller, K. Horn, and R. Bennewitz, *Phys. Rev. Lett.*, 2009, **102**, 086102.

16. Y. J. Shin, R. Stromberg, R. Nay, H. Huang, A. T. S. Wee, H. Yang, and C. S. Bhatia, *Carbon N. Y.*, 2011, **49**, 4070–4073.

17. P. Egberts, G. H. Han, X. Z. Liu, A. T. C. Johnson, and R. W. Carpick, *ACS Nano*, 2014.

18. T. Yoon, W. C. Shin, T. Y. Kim, J. H. Mun, T.-S. Kim, and B. J. Cho, *Nano Lett.*, 2012, **12**, 1448–52.

19. X.-Z. Liu, Q. Li, P. Egberts, and R. W. Carpick, *Adv. Mater. Interfaces*, 2014, **1**.

20. X. Wang, H. You, F. Liu, M. Li, L. Wan, S. Li, Q. Li, Y. Xu, R. Tian, Z. Yu, D. Xiang, and J. Cheng, *Chem. Vap. Depos.*, 2009, **15**, 53–56.

21. W. Liu, H. Li, C. Xu, Y. Khatami, and K. Banerjee, *Carbon N. Y.*, 2011, **49**, 4122–4130.

22. Y. Zhang, T. Gao, Y. Gao, S. Xie, Q. Ji, K. Yan, H. Peng, and Z. Liu, *ACS Nano*, 2011, **5**, 4014–4022.

23. L. Gao, J. R. Guest, and N. P. Guisinger, *Nano Lett.*, 2010, **10**, 3512–6.

24. W. Zhu, T. Low, V. Perebeinos, A. a Bol, Y. Zhu, H. Yan, J. Tersoff, and P. Avouris, *Nano Lett.*, 2012, **12**, 3431–6.

25. L. Zhao, K. T. Rim, H. Zhou, R. He, T. F. Heinz, a. Pinczuk, G. W. Flynn, and a. N. Pasupathy, *Solid State Commun.*, 2011, **151**, 509–513.

26. D. Yoon, Y. Son, and H. Cheong, 2011, 3227–3231.

27. D. Nix, F.C. and MacNair, *Phys. Rev. B*, 1941, **60**, 597.

28. J. Cho, L. Gao, J. Tian, H. Cao, W. Wu, Q. Yu, and E. N. Yitamben, 2011, 3607–3613.

29. J. Tian, H. Cao, W. Wu, Q. Yu, N. P. Guisinger, and Y. P. Chen, *Nano Lett.*, 2012, **12**, 3893–9.

30. S. D. Costa, A. Righi, C. Fantini, Y. Hao, C. Magnuson, L. Colombo, R. S. Ruoff, and M. A. Pimenta, *Solid State Commun.*, 2012, **152**, 1317–1320.

31. J. Bai, X. Zhong, S. Jiang, Y. Huang, and X. Duan, *Nat. Nanotechnol.*, 2010, **5**, 190–4.

32. Y. Wang, Y. Shao, D. W. Matson, J. Li, and Y. Lin, *ACS Nano*, 2010, **4**, 1790–1798.

33. M. Wojtaszek, N. Tombros, a. Caretta, P. H. M. van Loosdrecht, and B. J. van Wees, *J. Appl. Phys.*, 2011, **110**, 063715.

34. D. G. Matei, N.-E. Weber, S. Kurasch, S. Wundrack, M. Woszczyna, M. Grothe, T. Weimann, F. Ahlers, R. Stosch, U. Kaiser, and A. Turchanin, *Adv. Mater.*, 2013, **25**, 4146–51.

35. A. Zandiatashbar, G.-H. Lee, S. J. An, S. Lee, N. Mathew, M. Terrones, T. Hayashi, C. R. Picu, J. Hone, and N. Koratkar, *Nat. Commun.*, 2014, **5**, 3186.

36. G. N. Taylor and T. M. Wolf, *Polym. Eng. Sci.*, 1980, **20**, 1087–1092.

37. a. C. Ferrari, J. C. Meyer, V. Scardaci, C. Casiraghi, M. Lazzeri, F. Mauri, S. Piscanec, D. Jiang, K. S. Novoselov, S. Roth, and a. K. Geim, *Phys. Rev. Lett.*, 2006, **97**, 187401.

38. V. Yu, E. Whiteway, J. Maassen, and M. Hilke, *Phys. Rev. B*, 2011, **84**, 205407.

39. J. D. Jones, W. D. Hoffmann, a. V. Jesseph, C. J. Morris, G. F. Verbeck, and J. M. Perez, *Appl. Phys. Lett.*, 2010, **97**, 233104.

40. I. Pocsik, M. Hundhausen, M. Koos, and L. Ley, *J. Non. Cryst. Solids*, 1998, 1083–1086.

41. Z. Sun, Z. Yan, J. Yao, E. Beitler, Y. Zhu, and J. M. Tour, *Nature*, 2010, **468**, 549–52.

42. F. Tuinstra and J. L. Koenig, *J. Chem. Phys.*, 2003, **53**, 1126–1130.

43. O. Akhavan, *Carbon N. Y.*, 2010, **48**, 509–519.

44. J. S. Bunch, S. S. Verbridge, J. S. Alden, A. M. Van Der Zande, J. M. Parpia, H. G. Craighead, and P. L. Mceuen, *Nano Lett.*, 2008, **8**, 2458–2462.

 This journal is © The Royal Society of Chemistry 2014

45. J. Iijima, J.-W. Lim, S.-H. Hong, S. Suzuki, K. Mimura, and M. Isshiki, *Appl. Surf. Sci.*, 2006, **253**, 2825–2829.

46. A. Ferrari and J. Robertson, *Phys. Rev. B*, 2000, 61, 14095–14107.

47. a. Siokou, F. Ravani, S. Karakalos, O. Frank, M. Kalbac, and C. Galiotis, *Appl. Surf. Sci.*, 2011, **257**, 9785–9790.

48. K. N. Kudin, B. Ozbas, H. C. Schniepp, R. K. Prud'homme, I. a Aksay, and R. Car, *Nano Lett.*, 2008, **8**, 36–41.

49. L. M. Malard, M. a. Pimenta, G. Dresselhaus, and M. S. Dresselhaus, *Phys. Rep.*, 2009, **473**, 51–87.

50. Y. Y. Wang, Z. H. Ni, T. Yu, Z. X. Shen, H. M. Wang, Y. H. Wu, W. Chen, and A. T. S. Wee, *J. Phys. Chem. C*, 2008, **112**, 10637–10640.

51. Y. Shao, S. Zhang, M. H. Engelhard, G. Li, G. Shao, Y. Wang, J. Liu, I. a. Aksay, and Y. Lin, *J. Mater. Chem.*, 2010, **20**, 7491.

52. M. Lenglet, K. Kartouni, J. Machefert, J. M. Claude, P. Steinmetz, E. Beauprez, J. Heinrich, N. Celati, A. De Spectroscopic, D. Traitement, D. Surface, U. De Rouen, M. Saint, A. Cedex, L. D. C. Mi, U. D. N. I, and F. Sciences, *Mater. Res. Bull.*, 1995, **30**, 393–403.

53. G. Diankov, M. Neumann, and D. Goldhaber-Gordon, *ACS Nano*, 2013, **7**, 1324–32.

54. V. M. Donnelly and A. Kornblit, *J. Vac. Sci. Technol. A Vacuum, Surfaces, Film.*, 2013, **31**, 050825.

55. J. T. Herron and D. S. Green, *Plasma Chem. Plasma Process.*, 2001, **21**.

56. C. Cardinaud, M. Peignon, P. Tessier, and L. Materiaux, *Appl. Surf. Sci.*, 2000, **164**, 72–83.

57. D. L. Manos, D.M. Flamm, *Plasma Etching, and Introduction*, 1989.

58. C. Riccardi, R. Barni, and M. Fontanesi, *J. Appl. Phys.*, 2001, **90**, 3735.

59. a Hojabri, N. Haghighian, K. Yasserian, and M. Ghoranneviss, *IOP Conf. Ser. Mater. Sci. Eng.*, 2010, **12**, 012004.

60. N. Cabrera and N. Mott, *Reports Prog. Phys.*, 1949.

61. T. N. Rhodin, *J. Am. Chem. Soc.*, 1950, **72**, 5102–5106.

62. Z. Ye, C. Tang, Y. Dong, and A. Martini, *J. Appl. Phys.*, 2012, **112**, 116102.

[a] *Department of Engineering Physics, Mcmaster University, Hamilton, Ontario, Canada L8S 4L7*
[b] *Department of Physics, McGill University, Montr´eal, Canada H3A 2T8*